Applied Optics (Lasers, Photonics, and Environmental Optics) 36 (24) 6149-6156, 1997

A Neural Network Based Spatial Light Scattering Instrument for Hazardous Airborne Fiber Detection

AUTHORS:

Paul Kaye, Edwin Hirst, and Zhenni Wang-Thomas.

AFFILIATION:

Engineering Research and Development Centre

University of Hertfordshire

Hatfield, Hertfordshire, AL10 9AB, U.K.

ABSTRACT

A laser light scattering instrument has been designed to facilitate the real-time detection of potentially hazardous respirable fibers, such as asbestos, within an ambient environment. The instrument captures data relating to the spatial distribution of light scattered by individual particles in flow using a dedicated multi-element photodiode detector array. These data are subsequently processed using an artificial neural network which has previously been trained to recognise those features or patterns within the light scattering distribution which may be characteristic of the specific particle types being sought, such as for example, crocidolite or chrysotile asbestos fibers. Each particle is thus classified into one of a limited set of classes based upon its light scattering properties, and from the accumulated data a particle concentration figure for each class may be produced and updated at regular intervals. Particle analysis rates in excess of 10^3 per second within a sample volume flow-rate of 1 litre per minute are achievable, offering the possibility of detecting fiber concentrations at the recommended maximum exposure limit of 0.1 fibers/ml within a sampling period of a few seconds.

KEY WORDS:

Light scattering; Fibers; Asbestos; Neural Networks.

INTRODUCTION

The in-situ detection of potentially hazardous respirable fibers has become a growing concern within industrialised countries as the health risks associated with these fibers have become more fully understood. The most commonly encountered hazardous fibers are of asbestos materials which, despite a widespread ban on their use for many years, are still present in vast quantities in public and commercial buildings and plant throughout the world. The most abundant asbestos mineral, chrysotile (or white) asbestos, is present in over 95% of these installations. The second most commonly found variety is crocidolite (or blue) asbestos, with amosite (or brown) asbestos being a third but much rarer form. Scanning electron micrographs of crocidolite and chrysotile materials are shown in Figure 1. Crocidolite and amosite belong to the amphibole class and are characterised by the fine, straight, needle-like fibers produced when the material is fragmented. Chrysotile asbestos belongs to the serpentine class of minerals and is characterised by a natural curvature in the fibers it produces. All three materials produce fibers which are capable of penetrating deep into the lung and which, because of their shape, become entrapped there. Crocidolite and amosite fibers are known to be far more carcinogenic than those of chrysotile asbestos, and though the exact reasons for this are still not confirmed, the half-life of the fibers in the lung (a function of the body's ability to chemically dissolve the fibers) is believed to play a major role[1] since this may be measured in decades for amphibole fibers compared to months for chrysotile fibers.

The recent *Lancet* paper by Peto *et al* [2] discussing the continuing increase in mesothelioma mortality in Britain has highlighted once again the potential hazard of respirable asbestos fibers generated during clearance operations or routine building maintenance work. Indeed, the high rates of disease associated with asbestos inhalation resulted in the statement in 1990 by the US National Institute for Occupational Safety and Health (NIOSH) that there is "no evidence for a threshold or 'safe' level of asbestos exposure".[3]

Airborne Fiber Measurement

The most commonly used method for assessment of airborne fiber concentrations is via filter cassette sampling followed by phase contrast light microscope (PCM) counting of fibers. Stringent counting rules are laid down in standards such as NIOSH 7400[4] which detail the size and aspect ratios of particles to be counted as fibers, and define how to deal with inevitable occurrences of crossed fibers, fibers attached to other particles, and fibers lying partly outside the measurement template. In the NIOSH standard, only particles greater than 5µm length with an aspect ratio greater than 3:1 are counted as fibers, whilst fibers with a diameter greater than 3µm or which are attached to other particles greater than 3µm diameter are not counted. The counting processes are laborious and expensive to perform, and perhaps most importantly, provide results only many hours after the sampling (and possible inadvertent exposure of personnel) has occurred. Numerous attempts have therefore been made by other researchers to address methods by which real-time or in-situ detection of airborne asbestos and other potentially hazardous fibers may be achieved.

A well established instrument for airborne fiber measurement is the FAM-7400 Fibrous Aerosol Monitor (Mie Inc., Bedford, Massachusetts) developed originally by Lilienfeld *et al*.[5] in 1979. This instrument draws air containing the airborne particles through a laser scattering chamber which is enveloped by a quadruple electrode arrangement. By applying a time varying signal to the electrodes, the electric field within the scattering chamber causes conducting fibers present in the air to oscillate. (Asbestos fibers generally fall into this category because of their high water adsorption). The consequent cyclic variation in light scattered by the fibers to a single light detector at the side of the chamber is used to assess fiber concentration in the air. The FAM-7400 is capable of detecting individual fibers within the scattering chamber though the geometry of its detection volume may lead to comparatively high coincidence losses, typically ~15% at a measured concentration of 15 fibers/ml.[6] Its comparatively low sample throughput may also lead to prolonged sampling times. For example, counting 10 fibers at the US Occupational Safety and Health Administration action limit of 0.1 fibers/ml for occupational exposure requires ~10 minutes sampling time.

More recently, Rood *et al* [7] have described a low cost portable fiber monitor developed at the UK Health and Safety Executive laboratories. This device is based on the differential light scattering produced by fibrous particles which are deposited electrostatically in uniform alignment onto a glass substrate. It is capable of detecting airborne asbestos fibers but is not designed to detect individual particles, relying instead on the summation of scattering signals from a multitude of deposited fibers in order to achieve a detectable signal. Rood states that the UK clearance limit for asbestos in buildings of 0.01 f/ml can be detected after about 300 minutes sampling time.

In theory, the detailed spatial intensity distribution of light scattered by individual particles (the *scattering profile*) contains information relating to the particle's size, its shape, and its orientation with respect to the incident illumination. It is also a function of the wavelength and polarization of the incident illumination. The research reported here has sought to exploit characteristic features of the scattering profiles of, primarily, chrysotile and crocidolite asbestos fibers, with the aim of facilitating the rapid discrimination of each type of fiber from other particles present within an ambient environment.

Spatial Laser Scattering Profiles

Scattering profiles from a wide variety of particle types have been studied by the authors to verify scattering characteristics, to aid the validation of theoretical models (see, for example, Hirst *et al* [8]), and to provide the basis for practical instruments for particle shape classification. Conventional optical scattering instruments used for particle counting and/or sizing normally rely on the collection of scattered light with a single discrete detector. Such instruments cannot provide information on particle shape, and indeed normally assume that all measured particles are spherical when ascribing a size value to them. When several detectors are used, each collecting light over a different solid angle within the sphere of scattering around the particle, some shape as well as size information is obtainable and this principle is embodied in an earlier instrument developed by the authors (Kaye *et al* [9]).

In order to extract more subtle information relating to particle morphology, the spatial intensity distribution of light scattered by the particle must be recorded in more detail. The exact configuration of detectors used to record this information is inevitably a compromise between the level of detail sought and the number of detectors, and hence data processing time, which can be tolerated. In order to establish an optimal detector configuration (in terms of number, geometry, etc.) for the desired analysis of asbestos fiber spatial scattering it was first necessary to record the spatial scattering profiles from these fibers and other particulates at sufficient resolution to allow detailed modelling to take place. This was achieve using a laser scattering test chamber which incorporated an intensified charge-coupled-device (CCD) camera to record scattering profiles from particles illuminated by a 5mW 670nm diode laser. This test chamber is shown schematically in Figure 2. In brief, airborne particles are drawn through the chamber in a sample airstream which is ensheathed in a layer of filtered air. These combined laminar flows are aerodynamically focused such that the sample air column passes through the central region of an incident laser beam, the beam being linearly polarized in the plane of the diagram. This focusing also has the effect of tending to align elongated particles with their long axis parallel to the axis of flow. The light scattered at angles from 5° to 30° to the beam axis and throughout 360° of azimuth is recorded by the CCD camera as the particle traverses the beam and this image is passed to a host computer for storage. The system is comparatively slow, recording and storing approximately two images per second.

Figure 3 shows examples of scattering profiles recorded from various particle types. The top row shows scattering profiles from a variety of ‘background’ particles: those of irregular shape (most commonly encountered); droplets; and regular crystalline shape (normally rare). The second and third rows show profiles recorded from crocidolite and chrysotile asbestos fibers respectively. The images illustrate the wide variety of scattering profiles which may be encountered from different particle morphologies as well as the preferential vertical orientation (and predominantly horizontal scattering) exhibited by the fibrous particles within the sample flow. The asbestos fiber measurements were

recorded from aerosols which had been produced from dry asbestos powders using UICC (Union Internationale de la research Contre le Cancer) reference materials. The signal dynamic range achievable by the instrument allowed capture of scattering profiles from fibers of length from a few microns to approximately 20µm, and thicknesses from ~0.25µm upwards.

As illustrated in Figure 3, the chrysotile and crocidolite fiber profiles showed some significant differences. The chrysotile fibers, being normally curved, caused the scattering profiles to assume a 'bow-tie' appearance where the scattering is still predominantly horizontal but the differing inclinations of incremental sections of fiber length to the incident illumination cause the fine divergent structure shown. The crocidolite material, in contrast, produces straight fibers of more regular morphology which result in extremely well defined horizontal scattering. The width of the horizontal scattering arms is inversely related to the aspect ratio of the fiber, with high aspect ratio fibers producing the thinnest scattering. In both chrysotile and crocidolite fibers, the fiber volume may be related to a first approximation to the total scattered light recorded.

The particle scattering profile examples given in figure 3 illustrate some of the morphology dependent features whose recognition and analysis may offer a potential route to particle classification. Additionally, the prospect of identifying asbestos-like fibers from background airborne particulates and of possibly discriminating between chrysotile fibers and crocidolite (and similar fiber types) is offered. This paper goes on to describe an instrument which seeks to exploit this opportunity.

DETERMINATION OF OPTIMAL DETECTOR GEOMETRY

The optimal design for the detector array to be used in the new instrument was determined by simulating the performance of a variety of possible configurations and assessing their performance in terms of particle discrimination efficiency and processing speed for a variety of different processing algorithms.

The computer simulation was achieved by mapping each possible detector design onto each of several thousand scattering profiles (similar to those shown in Figure 3) for various particle types recorded using the intensified camera system described earlier. Detector designs varied from a simple 8-element radial array to a 64-element array configured in non-uniform offset rings. For each element of an array, the simulated scattered light signal was determined by integration over the corresponding area of the scattering profile image. The simulated detector outputs for each detector array geometry were then passed for analysis to each of four commonly used data classification methods: Normal Distribution, Linear Discriminant, k-Nearest Neighbours, and Radial Basis Function neural network. (The detailed operation of these classification algorithms is not given here, and the interested reader is directed to one of the many excellent texts on classification theory, for example *Pattern Classification and Scene Analysis*[10], for more information). Each of the classification methods required the presence of 'class templates' against which the incoming particle data could be compared and subsequently classified. These templates were computed for each detector geometry from a base of typically 100 images from each of chrysotile fiber scattering profiles, crocidolite profiles, and randomly selected profiles recorded from background airborne particulates, (see Discussion section). Up to ten thousand scattering profile images recorded from known aerosols of each particle type were subsequently analysed by each of the four classification methods and for each of the detector array geometries. This allowed the determination of the specific combination of detector geometry and classification method which yielded optimal particle classification accuracy and speed of execution within the constraints of conventional personal computer processing performance.

Detector Configuration and Classification Algorithm

The outcome of this simulation exercise established that the detector geometry shown in Figure 4, in combination with the RBF neural network classification method, gave optimal particle classification performance. The 33-element detector array comprised two annular rings, labelled A and B in Figure 4, each divided into 16 detector elements. These surrounded a center annular ring, labelled C, which could be used in conjunction with the other detector elements to estimate a spherical equivalent

particle size (from Mie theory[11]). The concentric ring detectors A and B provide the spatial scattering data required for particle classification. The ring offset was to minimize the possibility of fine fiber scattering from elongated fibers lying entirely along the 'dead-zones' between adjacent detector elements in both the A and B segmented rings.

The Radial Basis Function network is arguably one of the simplest forms of artificial neural network. It is based on the use of 'training' data, in our case these being example sets of 100 scattering patterns from each of the particle classes we wish to discriminate. The training data result in defined regions of mathematical hyperspace corresponding to the chosen classes. When new data (expressed as an *input vector*) derived from to an unknown particle is input to the network, the network evaluates the 'distance' between this input vector and its predefined class data regions and indicates to which class the unknown particle corresponds most closely.

The RFB network has an architecture consisting of only one hidden layer, as illustrated in Figure 5. In our case, the inputs, labelled x_1 to x_n were the values of the light scattering data from either the A or B detector ring; these were processed independently through the network so as to allow a voting on the classification outcome. Only if both processes resulted in the same classification for a particle (judged as that having the highest linear summation output value) was the particle ascribed to that class (shown as *class1, class2,* etc. in Figure 5). If there was a discrepancy in classification results from the two detector rings the particle was classified into the lower of the two classes.

The hidden nodes ω_1 to ω_n are radial basis functions that take the form

$$\omega_i\left(\left\|\mathbf{x}-\mathbf{x}_i\right\|\right) \tag{1}$$

where $\omega_i(\bullet)$ is a non-linear function of the distance between the input vector **x** (based on the detector ring values for the unknown particle) and the ith center vector $\mathbf{x}_i$ (marking the hyperspace region corresponding to each prescribed class of particle). The network output vector **class** is simply the linear summation of the weighted basis functions

$$class_j = \sum_{i=1}^{n} w_{ji}\omega_i(\|\mathbf{x} - \mathbf{x}_i\|), \quad j = 1,2,...,k \tag{2}$$

the weights for each class w_{11}, w_{21}, ...to w_{kn} having been established by the training data.

In our case, the radial basis functions were chosen to be Gaussian, a commonly used approach and one which gave good classification results. The functions were of the form

$$\omega_i(\|\mathbf{x} - \mathbf{x}_i\|) = e^{-\frac{\|\mathbf{x}-\mathbf{x}_i\|^2}{d^2}} \tag{3}$$

where *d* is a constant bandwidth parameter.

Figure 6 summarises the simulated classification performance of the selected detector geometry and RBF analysis method. Some ten thousand examples of scattering profiles recorded from known aerosols of each of the three chosen particle types (chrysotile; crocidolite; and background) were processed and classified into their respective classes. Ideally, 100% of each input test data type should be classified into its correct particle class. In practice, over 99% of background particles were correctly classified as background, with 0.1% being mis-classified as chrysotile particles and 0.6% mis-classified as crocidolite. These mis-classification figures are as a result of non-asbestos fibers within the background sample producing scattering profiles sufficiently similar to the extremes of the chrysotile or crocidolite classes that they were classified as such. They therefore represent a threshold level against which actual fiber concentration measurements must be compared. Similarly, over 80% of crocidolite and 70% of chrysotile particles were correctly classified. The mis-classification of the remainder of these particles into the 'background' class is inevitable using this laser scattering technique since some crocidolite or chrysotile particles are aerosolised as irregular clumps or fiber aggregates which do not produce characteristic fiber scattering. The consequence will be the underestimation of the true asbestos fiber concentration by some small margin, though this parallels the decision processes which occur during the standard PCM filter sample counting technique (see Discussion section).

INSTRUMENTATION

The new fiber characterisation instrument incorporates the selected detector geometry as a custom photodiode array chip, manufactured by Centronic Ltd., Croydon, England. The chip has a diameter of 11mm and is mounted into a commercial pin-grid-array package with no covering window. The complete instrument is shown schematically in Figure 7. The laser scattering chamber is similar in principle to that used with the intensified CCD camera system (Figure 2) with the exception that the low-power diode laser has been replaced with a high-power 100mW, 670nm wavelength diode laser (Power technology Inc., Little Rock, Arkansas) to compensate for the fact that the photodiode array has no inherent gain and would be incapable of providing adequate output signals if used with the low-power laser. (Again, the laser output is linearly polarized in the plane of the diagram). The beam cross-section at the intersection with the sample air flow is of ellipsoidal shape, approximately 2mm in width and 120µm depth, leading to a particle transit time through the beam of ~5µs. Sample airflow through the device is set to be 1 litre per minute. Since particle trajectories through the beam could take place anywhere within the horizontal cross-sectional area of the sample air column (approximately 1mm diameter), the scattered light capture optics were designed to ensure that such particle trajectory variation did not cause significant translation of the scattering profile image on the detector array. The center detector ring C receives light scattered between 4° and 10° to the primary beam axis; the second and third rings, B and A, receive light scattered between 10° and 18°, and 18° and 28° respectively.

The operation of the signal acquisition, digitization and buffering electronics is shown schematically in Figure 8. When a particle enters the laser beam the signal received from the central annular ring C begins to rise. This rise is detected by a particle trigger detection circuit which initiates data acquisition from the other 32 detector elements. This acquisition is achieved by two dedicated ASIC (application specific integrated circuit) chips, labelled HX2 in Figure 8. These chips are manufactured by Rutherford Appleton Laboratories, Didcot, UK. Each HX2 chip contains 16 parallel integrators which integrate the signals from the individual detector elements for the duration of the particle transit through the beam. The chips then hold these analog signal values and serially multiplex them out to

analog-to-digital converters. FIFO (First In First Out) buffers subsequently store the digital data, 33 values per particle, before transferring them at an optimal rate to the neural network data processing system (based on dual Motorola 68040 processors) for particle classification.

Figure 9 shows typical examples of the type of detector data fed to the neural network for analysis and pattern classification. The examples show typical scattering data recorded from a crocidolite fiber, a chrysotile fiber (both derived from the UICC reference materials referred to earlier), and an irregular shaped background particle. Examples similar to these constituted the class-template data used to 'train' the neural network. Data elements labelled 1-16 represent the output from the outer detector ring A, and those labelled 17-32 represent the output from the middle ring B; as a consequence crocidolite fiber scattering produces four sharp peaks, chrysotile produces four broad peaks, and the background particle produces an irregular pattern. The data have been normalised to the highest data element in each case. Note that the output from the 33rd element, the center ring C, which is used to provide an approximate assessment of particle size, is not shown in Figure 9. The output from this detector element does not normally form part of the neural network analysis since to do so could create the possibility of the particle classifications being unduly biased on the basis of particle size rather than shape (or, more correctly, scattering asymmetry).

In order to assess the performance of the machine neural network against results achieved by manual classification, experiments were carried out using aerosols containing mixed particle types. For each aerosol, data relating to three thousand particles were classified, firstly by visual inspection using a trained volunteer and secondly by use of the RBF neural network classifier. The data were of the form similar to that shown in figure 9. Since these mixed aerosols contained crocidolite, chrysotile, and background particles and it was known that some overlap in the scattering characteristics of these materials was inevitable (as illustrated in Figure 6), the classifications used were *High-risk Fibers* (those which displayed predominantly crocidolite-like scattering features), *Medium-risk Fibers* (those which displayed predominantly chrysotile-like scattering features), and *Other Particles.* Table

1 summarises the results for one such mixed aerosol, illustrating the close similarity in classification performance between machine and manual classifications; the significant difference being that the manual classification required several hours (similar to that required for PCM fiber counting on filters), whilst the machine classification required only seconds.

DISCUSSION

The established method of fiber contamination assessment using filter sampling followed by phase contrast microscopy is known to have disadvantages in terms of the prolonged analysis time required and the inevitable subjectivity in the counting introduced by each individual microscopist. Nevertheless it remains the standard method by which all other methods will be judged. Despite its near real-time response, the light scattering method described in this paper would gain acceptance only if the results it gave were close to those which the standard method would have given under similar measurement conditions. The authors are therefore currently undertaking a series of field experiments in actual asbestos clearance operations during which measurements are taken using both the standard filter method and the light scattering technique to allow such comparisons to be made. Here the use of a neural network provides a useful means of tuning the output of the classification process so as to bring it into line with that of a microscopist using filter analysis. With phase contrast imaging microscopy of filter samples there exists a continuum of possible fiber presentations (crossed fibers, multiple-fibers, fibers attached to other particles, etc.) about which the microscopist must make a decision. Similarly, in the case of the light scattering data presented to the neural network there exists a continuum of scattering patterns (similarly due to single fibers, multiple-fibers, fibers attached to other particles, etc.) about which the neural network computes a decision based upon its training template data. For example, a microscopist may exclude a fiber because it has attached to it a comparatively large non-fibrous particle; similarly, the neural network would reject the scattering pattern from such a composite particle because of the severe perturbation from ideal fiber scattering which the sub-particle would cause. Thus, by appropriate selection of the training template data, the breadth of light scattering patterns which the neural network regards as, say, hazardous fibers, may be

adjusted so as to be in accord with that produced by the trained microscopist assessing fiber images on a filter substrate. If this process is successfully achieved, the light scattering method could provide a valuable real-time alternative to filter sampling fiber contamination assessment.

ACKNOWLEDGEMENTS

This work has been supported by grants from the UK Engineering and Physical Sciences Research Council and Department of Trade and Industry. The asbestos fiber aerosol measurements were made at the Medical Research Council's Toxicology Laboratories, Leicester, U.K., under the direction of Dr J. A. Hoskins.

REFERENCES

1. R.C. Brown, J. A. Hoskins, and N. F. Johnson, eds., Mechanisms in fiber carcinogenesis. Life Science Vol. 223, (Plenum press. New York, 1991), pp 1-589.
2. J. Peto, J.T. Hodgson, F.E. Matthews, and J.R. Jones, "Continuing increase in mesothelioma mortality in Britain". The Lancet. 345, March 4, 535-539 (1995).
3. Testimony of NIOSH on occupational exposure to asbestos, tremolite, anthrophyllite and actinolite. 29CFR, Parts 1910 and 1926. 9 May, 1990.
4. J. Carter, D. Taylor, and P.A. Baron, "Fibers Method 7400 revision no.3:5/15/89" in NIOSH Manual of Analytic Methods, Cincinnati, OH: DHHS/NIOSH.
5. P. Lilienfeld, P. Elterman, and P. Baron , "Development of a prototype fibrous aerosol monitor". A. Ind. Hyg. Assoc. J. 40, 4, 270-282 (1979).
6. P.A. Baron, M.K. Mazumder, and Y.S. Cheng, "Direct reading Techniques using Optical Particle Detection" in Aerosol Measurement, K. Willeke and P.A. Baron, eds., (Van Nostrand Reinhold, New York, 1993), pp. 403-408.
7. A.P. Rood, E.J. Walker, and D. Moore, "Construction of a portable fibre monitor measuring the differential light scattering from aligned fibres" in Proceedings of the International Symposium: Clean Air at Work, R.H. Brown, M. Curtis, K.J. Saunders, and S. Vandrendreissche, eds. (Royal Soc. of Chemistry, London, 1992), pp.265-267.
8. E. Hirst, P.H. Kaye, and J. Guppy, "Light Scattering from Non-spherical Airborne Particles; experimental and theoretical comparisons", Appl. Opt. 33, 30, 7180-7186 (1994).
9. P.H. Kaye, K. Alexander-Buckley, E. Hirst, and S. Saunders "A Real-time Monitoring System for Airborne Particle Shape and Size Analysis", J. Geophysical Res. (Atmospheres), 101, D14, 19,215-19,221 (1996).
10. R.O. Duda and P.E. Hart, Pattern Classification and Scene Analysis, (Wiley Interscience, 1973).

11. C.F. Bohren and D.R. Huffman, Absorption and Scattering of Light by Small Particles. (Wiley, New York, 1983).

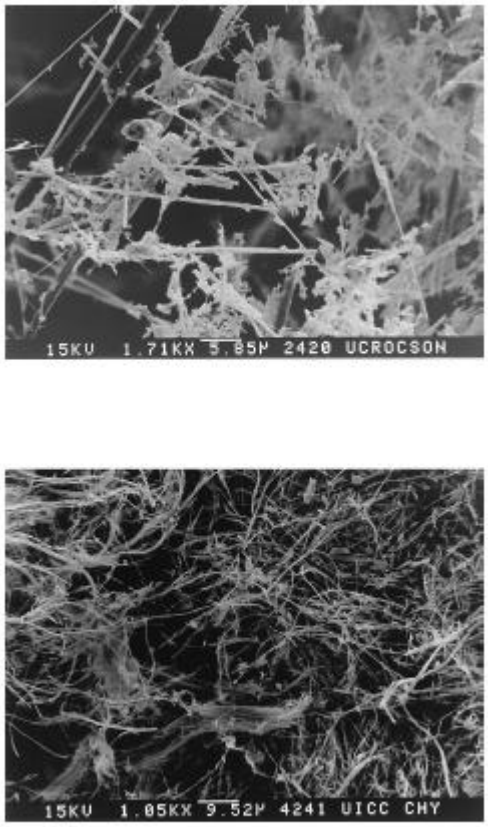

Fig. 1. Scanning electron micrographs of crocidolite asbestos (top) and chrysotile asbestos (bottom) showing the characteristic needle-like and curved fibers, respectively. Fiber diameters range from submicrometer to a few micrometers.

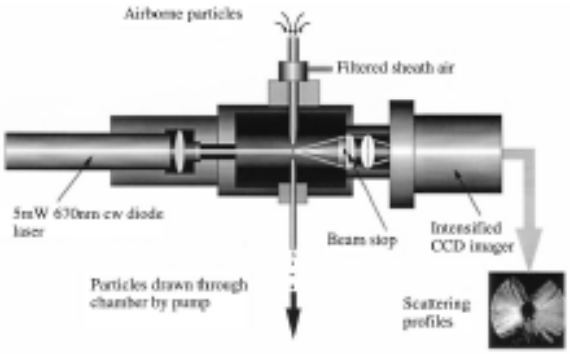

Fig. 2. Schematic diagram of the laser scattering test chamber used to collect high-resolution scattering profiles from individual particles carried in a sample airstream.

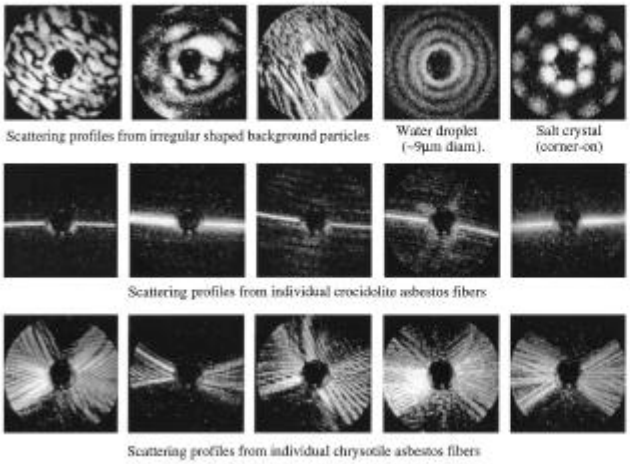

Fig. 3. Examples of scattering profiles recorded from individual airborne particles. The upper row illustrates the wide variety of profiles derived from typical background particles; the center row shows profiles from individual crocidolite asbestos fibers; and the lower row shows profiles from individual chrysotile asbestos fibers.

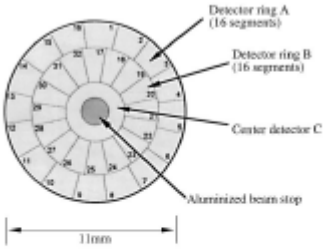

Fig. 4. Outline diagram of the layout of the custom multielement photodiode detector array used in the new instrument to collect light scattered from individual particles. The array is 11 mm in diameter and is configured on a single silicon substrate. The numbers that appear in each detector element are given to aid comparison with the examples of actual light scattering data given in Fig. 9.

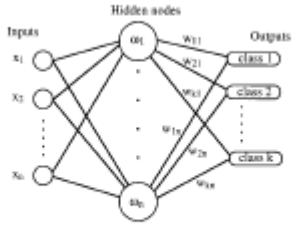

Fig. 5. Schematic illustration of the basic elements of a RBF neural network.

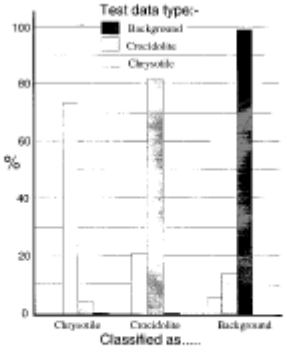

Fig. 6. Graphical representation of the simulated performance of the detector configuration (shown in Fig. 4) and the RBF neural network in terms of classifying particles from known aerosols. Ideally, 100% of each test data type should be classified into its correct class.

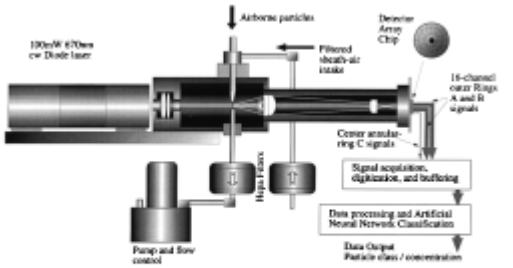

Fig. 7. Schematic diagram of the new laser scattering instrument that incorporates the custom photodiode detector array to collect light scattered from individual particles carried in the sample airstream.

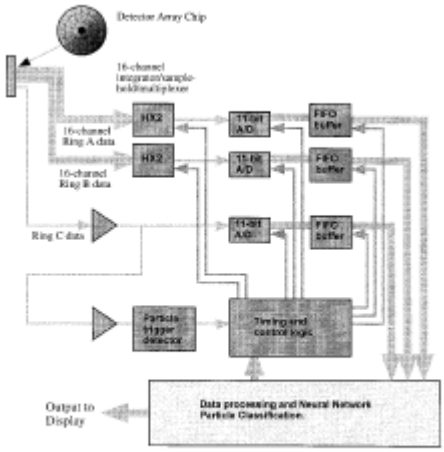

Fig. 8. Schematic diagram showing the acquisition and digitization process for light-scattering signals derived from the custom detector array chip.

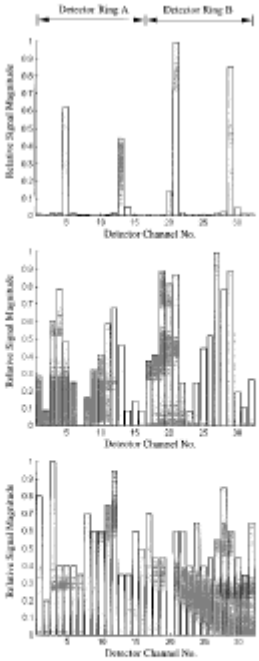

Fig. 9. Typical examples of the output of the detector system of the new instrument. These show the scattered light intensities received by each of the 32 detector channels (1–16 from the outer detector ring A and 17–32 from the middle ring B; refer to Fig. 4) for a single crocidolite asbestos fiber (top), a single chrysotile fiber (middle), and an irregular background particle. Data of this format are fed to the neural network for pattern classification.

TABLE 1

Particle Class	*Manual classification %*	*RBF Neural Network classification, %*
High-risk fibers	4.4	4.3
Medium-risk fibers	15.4	14.3
Other particles	80.2	81.4

Table 1 Summary of the classification of scattering profile data from a mixed aerosol containing crocidolite, chrysotile, and background particles. The classification was achieved both by visual inspection of graphical data (similar to those shown in Figure 9), and by RBF neural network analysis. High-risk fibers are those which display crocidolite-like scattering profiles; Medium-risk fibers are those which display chrysotile-like scattering.